IOP PUBLISHING PLASMA PHYSICS AND CONTROLLED FUSION

Plasma Phys. Control. Fusion **49** (2007) 1747–1766 doi:10.1088/0741-3335/49/11/001

Suprathermal deuterium ions produced by nuclear elastic scattering of ICRH driven He^3 ions in JET plasmas

F S Zaitsev[1], A Gondhalekar[2], T J Johnson[3], S E Sharapov[2], D S Testa[4], I I Kurbet[1] and JET EFDA contributors[5]

[1] Moscow State University, Faculty of Computational Mathematics and Cybernetics, 119992 Moscow, Russian Federation
[2] EURATOM/UKAEA Fusion Association, Culham Science Centre, Abingdon, OX14 3DB, UK
[3] Association EURATOM-VR, Alfven Laboratory, Royal Institute of Technology, 10044 Stockholm, Sweden
[4] CRPP, Association EURATOM - Confederation Suisse, EPFL, Lausanne, Switzerland

E-mail: zaitsev@cs.msu.su

Received 18 May 2007, in final form 27 August 2007
Published 24 September 2007
Online at stacks.iop.org/PPCF/49/1747

Abstract

Measurements of the suprathermal tail of the energy distribution function of deuterium ions, in plasmas containing MeV energy ICRH driven minority He^3 ions and majority deuterium ions, revealed that the suprathermal tail ion density exceeded by nearly an order of magnitude that expected due to nuclear elastic scattering (NES) of He^3 projectile ions on deuterium target ions. The experiments were performed on the Joint European Torus (JET), measurements of the line-of-sight integrated energy distribution functions of He^3 and suprathermal deuterium ions were made using a high energy neutral particle analyzer. The NES or 'knock-on' deuterium ion energy distribution function was simulated using the FPP-3D Fokker–Plank code (Zaitsev *et al* 2002 *Nucl. Fusion* **42** 1340) which solves the 3D trajectory averaged kinetic equations in JET tokamak geometry while taking into account NES of He^3 ions on the deuterium ions. The required input energy distribution function of ICRH driven He^3 ions was simulated using the SELFO code (Hedin *et al* 2002 *Nucl. Fusion* **42** 527). The comparison between measurement and simulation in the He^3 ICRH experiments is contrasted with an analogous previous comparison between measurements and simulation of JET plasmas in which 3.5 MeV DT fusion alpha-particles were the projectile ions, where measurement and simulation roughly agreed. Possible explanations for the observed excess knock-on deuterium tail in the experiments with He^3 minority

[5] See appendix of Watkins M *et al* 2006 *Proc. 21st IAEA Conf. on Fusion Energy 2006 (Chengdu, 2006)* (Vienna: IAEA).

ICRH are discussed. The importance of $D + He^3$ fusion products as additional drivers of suprathermal fuel ions is underlined.

(Some figures in this article are in colour only in the electronic version)

1. Introduction

The formation of suprathermal fuel ions due to nuclear elastic scattering (NES) between MeV energy minority fusion-born ions and majority thermal fuel ions is an intrinsic property of fusion plasmas. The possibility of obtaining information about DT fusion alpha-particles in tokamak plasmas by measuring the suprathermal tail of the energy distribution function of heavy impurity ions such as iron, formed due to NES on the alpha-particles, was first discussed in [1]. This formalism was further elaborated and extended in [2] to consideration of minority ICRH driven ions in the plasmas, where it was shown how the velocity-space anisotropy of the ICRH driven ions could also be exploited for diagnostic purposes. First measurements of the suprathermal tail of the deuterium ion energy distribution function, formed due to NES on 3.5 MeV DT fusion alpha-particles were reported on Joint European Torus (JET) [3]. Measurements of the line-of-sight integrated energy distribution function (LID) of deuterium ions were made using a high energy neutral particle analyzer (NPA), which revealed a population of MeV energy deuterium ions in the plasma. Comparison of the deduced energy distribution function of suprathermal deuterium ions with calculations, based on simplifying assumptions of confinement of DT fusion alpha-particles in the JET tokamak plasma and their classical slowing-down by Coulomb collisions with electrons and NES on majority fuel ions, showed that the two were in rough agreement. It was shown in [3] that the fusion alpha-particle energy distribution function as well as other details, such as the anisotropy of the alpha-particle distribution function, could be deduced from such NPA measurements of suprathermal deuterium and tritium ions. Subsequently, a neutron spectroscopy measurement of the effect of NES on total neutron emission in JET, using the same high fusion reactivity plasma pulses used for the NPA measurements of [3], was reported in [4]. A high-sensitivity magnetic proton recoil spectrometer measured the energy distribution function of the total neutron emission in the energy range 13.5–15.2 MeV. Comparison of the measurement and simulation identified part of the neutron emission spectrum as being due to fusion of suprathermal deuterium and tritium ions. Conclusions in [4] reinforce those drawn by the authors of the NPA measurements in [3]. For the full interpretation of the NPA measurements and elucidation of the underlying processes, a formalism suitable for full numerical simulation of the NPA measurements, in tokamak field geometry and including the NES effect, was developed in [5], implementing earlier theoretical formulations given in [1,2]. A successful comparison was made in [5] between the NPA measurements of the LID of suprathermal tail of deuterium ions and simulation of the tail, in JET geometry and using the measured plasma parameters.

NPA measurements like those discussed in this paper have become well established in JET for the measurement of the behaviour of MeV energy ions due to ion cyclotron resonance frequency heating and fusion reactions. Different aspects of behaviour of energetic ions have been studied: (1) neutralization of hydrogen and helium isotope ions by the main intrinsic impurities in JET plasmas and determination of the absolute ion energy distribution function [6], (2) interpretation of the fast ion energy content of the plasma [7, 11], (3) pinching of trapped ions [8], (4) suppression of velocity-space diffusion during ICRH [9], (5) simultaneous multi

hydrogen isotope ICRH [10], (6) DT and pT fusion [3, 12] and (7) radial redistribution of ICRH driven trapped ions due to kink instability [13]. The NPA measurements reported therein are line-of-sight integrated along the Z-axis. However, the ICRH driven high energy ion population giving rise to the atomic flux measured by the NPA is generated, confined and localized in the plasma core. The deduced ion energy distribution function of ICRH driven ions is therefore local, pertaining to the plasma core. References [7, 11] demonstrate how the total energy content of the MeV energy ion population may be deduced from the NPA measured absolute energy distribution function of ICRH driven ions, and that it was found to be in agreement with an independent determination of the same quantity deduced from measurements of plasma diamagnetism. This agreement supports modelling of ICRH which shows good focusing of applied RF power in the plasma core [7]. As for DT fusion alpha-particles and NES driven deuterons measured during DTE1, localization of the ions in the plasma core is assumed; this is reasonable because the source of the pertinent ions is the high temperature high fusion reactivity plasma which is located in the plasma core, as evidenced by the measured radial profiles of ion and electron temperatures and of neutron emissivity.

In order to investigate in depth plasmas with He^3 minority ICRH, which is the preferred main heating scheme on ITER, very detailed experiments and measurements were carried out on JET plasmas using this heating scheme. During these experiments the LIDs of He^3 ions and the deuterium ions were measured in the MeV energy range using the NPA and the analysis methods described in detail in [6]. In this paper we present a model for ICRH of He^3 ions in deuterium plasmas and a model for neoclassical ion transport in JET plasmas including NES. These are used to simulate the suprathermal tail of the deuterium ion energy distribution function and the LID in the measurement geometry. A comparison between the LID inferred from the NPA measurements and the simulation of it reveals an excess knock-on deuteron population in the measurement. A brief description is given of previous analogous comparison in which MeV energy DT fusion alpha-particles were the projectile ions, where no discrepancy was observed. Possible reasons for the discrepancies observed in the He^3 ICRH experiments are discussed.

The main differences between the two experiments, one with ICRH driven He^3 ions as the projectile, and the previous one in which DT fusion alpha-particles were the projectile are

(i) the energy distribution function of ICRH driven He^3 ions is strongly anisotropic in velocity space, whereas the DT fusion alpha-particle energy distribution function is relatively close to isotropic in velocity.
(ii) The energy distribution function of DT fusion alpha-particles did not reach steady state, while the plasmas with ICRH of He^3 ions were of sufficient duration for both the He^3 ion energy distribution and the NES driven suprathermal tail of the deuterium ion energy distribution function to reach steady state.
(iii) The high energy NPA used in the two measurements precluded separation of ions with the same charge-to-mass ratio. In consequence, measurement of the knock-on suprathermal deuterium ion tail in the DT experiments was contaminated with a small alpha-particle contribution as discussed in [3]. In contrast, in the ICRH experiments, the deuterium and He^3 atomic flux to the NPA were well separated.
(iv) In contrast to NES collision ($D + He^4$) the NES collision ($D + He^3$) has not only the NES branch, but also the well-known fusion branch

$$D + He^3 \rightarrow p(14.7\,\mathrm{MeV}) + He^4(3.6\,\mathrm{MeV}).$$

Among the differences listed above, the major unknown in the experiments under discussion here was the $D + He^3$ fusion yield, which was not measured. As we shall see later, the presence of this fusion branch may be the key feature distinguishing the experiments reported in this

paper from the earlier DT fusion experiments reported in [3]. ($D + He^3$) fusion in JET plasmas has been the subject of earlier investigations with He^3 minority ICRH [14], in experiments which were very similar to the present ones, apart from the high ICRH power applied and the high temperatures achieved. In the work reported in [14] the ($D + He^3$) fusion yield was deduced from measurements of γ-rays due to a secondary branch of the fusion reaction, $D + He^3 \rightarrow Li^3 + \gamma$ (16.6 MeV). In [14] a correlation was found between the ($D + He^3$) fusion power and the stored energy in the He^3 ion population. A high value for the fusion amplification factor $Q = P_{\text{fusion}}/P_{\text{ICRH}}$ of 1.25×10^{-2} was found. We shall see later by comparing figures 3 and 4, that there is a close correspondence in energy dependence between, on the one hand, the rate-coefficient for the main branch of the ($D+He^3$) fusion reaction and, on the other hand, the energy distribution function of the ICRH driven He^3 ions in JET, ensuring that fusion is by far the most dominant reaction between D and He^3 ions in JET plasmas.

The aim of this paper is to simulate the energy distribution function of suprathermal deuterium target ions in JET plasmas containing minority ICRH driven He^3 projectile ions and from this to calculate the LID of the suprathermal deuterium ions along the NPA line-of-sight and compare this with NPA measurements of the same quantity. Only NES of He^3 minority ions on deuterium majority ions is considered in the model; possible NES of ($D + He^3$) fusion-born alpha-particles and protons on the deuterium ions are ignored. In the modelling of NES of the anisotropic MeV energy He^3 ions on isotropic Maxwellian deuterium ions, cross-sections for close collision between He^3 projectile ion and D target ion given in [15] are used. A model of neoclassical ion transport accounting for large drift orbit widths, strongly non-Maxwellian distribution functions and toroidal geometry is incorporated in the Fokker–Planck FPP-3D code, including friction and diffusion in velocity space, pitch-angle scattering, non-circular geometry of the flux surfaces and time evolution of the plasma parameters. The FPP-3D code is described in full in [16–19]. FPP-3D code simulations have been bench marked against calculations with other tokamak codes: the BANDIT-3D code [22], the TRANSP code [23] and measurements [5]. The complexity of the NES problem considered here arises from the non-Maxwellian energy distribution function of the projectile He^3 ions and their strong velocity-space anisotropy and the very broad ion energy range encompassed by the NES process. The modified FPP-3D code incorporating NES has been benchmarked against the analytical formulation given in [2].

The distribution function of ICRH driven minority He^3 ions is simulated using the SELFO Monte-Carlo code [20]. The SELFO calculated energy distribution function of He^3 ions is used as an input to the FPP-3D code. For a qualitative analysis the SELFO + FPP-3D simulation is too complex, it is much faster and simpler to use an analytic approximation of the He^3 ion energy distribution function. For this we use the 'tail temperature' formulation of ICRH driven minority ions developed in [21].

The time dependent evolution of the knock-on tail was simulated in order to compute the maximum achievable NES driven perturbation of the deuterium ion energy distribution function, given a steady-state He^3 ion population. This is to be contrasted with an earlier [5] simulation of the suprathermal tail of the deuterium ion energy distribution function driven by NES on a non-steady-state DT fusion alpha-particle energy distribution function.

Section 2 presents the experimental set-up and the key plasma measurements which are used in the simulations. Section 3 describes modification of the FPP-3D neoclassical ion transport code to include a model for NES of MeV energy minority He^3 ions and the driving of the suprathermal tail of the majority ion energy distribution function. Section 3 also describes how the LID of the different ion species is constructed using FPP-3D. Section 4 gives a brief description of the SELFO code for simulation of the ICRH driven He^3 ion energy distribution function and a description of how to adapt the analytic formulation by Stix [21] for a

preliminary qualitative simulation of ICRH of minority ions. Section 5 presents the simulation, using the measured plasma parameters and using the models described in sections 3 and 4, of the neoclassical energy distribution function of the ICRH driven He^3 minority ions, and of the concomitant NES driven suprathermal tail of deuterium ions. From this simulation the LID of the two ion species is computed for comparison with the measurements. The comparison reveals that the FPP-3D code simulation underestimates by a factor of 10 the NES driven suprathermal tail of the deuterium ion energy distribution function. Section 6 gives a brief description of an earlier analogous comparison of measurement and simulation in which DT fusion alpha-particles were the projectile ions driving the suprathermal tail to the deuterium ions. Section 7 summarizes the main results of contrasting the comparisons in the two cases, drawing attention to an interpretation of the discrepancy between the simulation and measurement in the He^3 ICRH experiments. Implications for future work in ITER are mentioned.

2. The experimental set-up and plasma parameters

For measurement and analysis of NES effects in He^3 minority ICRH deuterium plasmas, a series of similar JET pulses (#53800, #53801, #53807, #53809, #53810, #53811) was used with a toroidal magnetic field $B(R_{\mathrm{mag}}) \approx 3.45$ T, toroidal plasma current $I_\phi \approx 1.8$ MA, major radius at the magnetic axis $R_{\mathrm{mag}} \approx 3$ m, plasma minor radius $\gamma_{\mathrm{a}} \approx 0.9$ m, elongation $\kappa \approx 1.5$ and some other parameters given in figures 1 and 2. Since the NPA could measure only one species of ion during one pulse, it was set up to measure He^3 ions in pulses #52800, #53801, #53807, #53809, and deuterium ions in pulses #53810, #53811. For the given magnetic field and ICRH frequency of 34 MHz, the fundamental He^3 ICRH resonance layer was located at $R_{\mathrm{ICRH}} \approx 3.08$ m (figure 2), while the fundamental hydrogen minority resonance was outside the plasma on the low-field side and the second harmonic hydrogen resonance (fundamental deuterium resonance) was close to the inner wall of the torus at $R \approx 2.3$ m. The vertical NPA line-of-sight in JET is located at major radius $R_{\mathrm{NPA}} = 3.07$ m, close to the magnetic axis and the ICRH resonance layer. As described in [3,6] the deduced LID is that of trapped ions with pitch-angle $\vartheta \approx \pi/2 \pm 5 \times 10^{-3}$ and with ion speeds $\upsilon_Z >> \upsilon_R$, $\upsilon_Z >> \upsilon_\phi$ and υ_Z/υ_R, $\upsilon_Z/\upsilon_\phi \geqslant 200$. In what follows, analysis of pulse #53807 (with measured LID of He^3 ions) and pulse #53810 (with measured LID of deuterium ions) is presented, as a representative of all the measurements made for this study.

Figure 1 shows the ICRH and NBI power waveforms and evolution of the main plasma parameters $T_{\mathrm{e}}(0)$, $T_{\mathrm{i}}(0)$ and $n_{\mathrm{e}}(0)$ in a JET pulse (#53807) which is representative of this series. The low power deuterium NBI was employed for spectroscopic measurements of ion temperature and plasma rotation. As described in [6] the NPA measurement of energetic hydrogen and helium isotope ions relies on charge-exchange with, respectively, one- and two-electron species of Be and C, the main intrinsic impurities in JET plasmas. The presence of NBI increases the density of Be and C charge donors, thereby improving the NPA measurement.

The density of He^3 ions is a critical parameter in the modelling of minority He^3 ICRH. In the experiments described, using available spectroscopic data, the He^3 ion density could be inferred only for the plasma edge. These measurements gave typically $n_{\mathrm{He}}/n_{\mathrm{e}} \leqslant 5\%$; for example in pulse #53810 $n_{\mathrm{He}}/n_{\mathrm{e}} \approx 4.8\%$. Considering that ICRH tends to expel resonant ions from the plasma core forming a hollow He^3 ion density profile, and that the edge helium density measurements yield the sum of He^3 and He^4 ion density, the measured value of $n_{\mathrm{He}}/n_{\mathrm{e}}$ mentioned above should be considered an overestimate of the actual core value of $n_{\mathrm{He}}/n_{\mathrm{e}}$. In the pulses used in this study $T_{\mathrm{e}}(0)/T_{\mathrm{d}}(0) \geqslant 2$, as seen in figure 1, thus the ICRH driven He^3 ions mostly heat electrons, indicating that the He^3 ion 'tail temperature' exceeds the critical

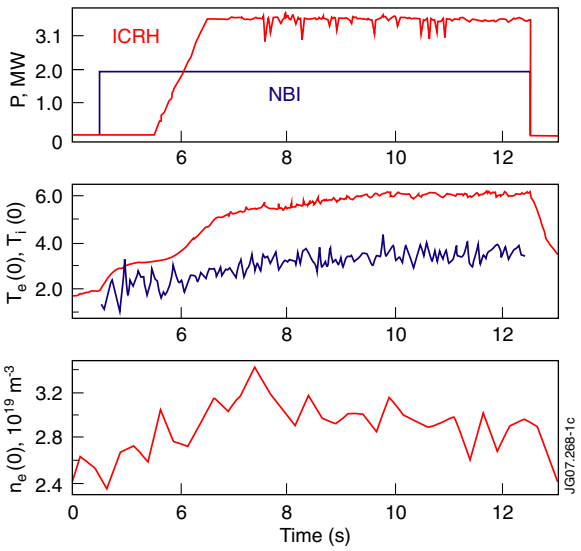

Figure 1. Evolution of key parameters for JET pulse #53807. Top box: waveform of applied ICRH and NBI heating power; middle box: on-axis electron temperature $T_e(0)$ measured using electron cyclotron emission (upper curve), and ion temperature $T_i(0)$ measured using charge-exchange spectroscopy (lower curve) keV; bottom box: on-axis electron density $n_e(0)$ measured using Thomson scattering. At t $\geqslant$9.5 s into the pulse $T_e(0)$, $T_i(0)$ and $n_e(0)$ are in steady state.

energy $E_{crit} \approx 28 \cdot T_e(0) \approx 170$ keV. Previous modelling studies of ICRH have shown that such a high 'tail temperature' for the He^3 ion energy distribution is achievable only for a He^3 ion density much lower than that given by the edge measurement mentioned above. Due to this uncertainty in the central density of He^3 ions a scan was performed, with $n_{He}/n_e = 3\%$, 2%, 1% and 0.5%, in the ICRH modelling in this study in order to infer a magnitude for n_{He_3}/n_e which would be closer to its actual central value.

Calculations show that within 0.5 s of the applied ICRH power reaching steady state the whole He^3 ion population has been accelerated to the full energy. It takes a further period corresponding to the slowing-down time of MeV energy He^3 ion, $\approx$1.5 s, for the electron heating to reach steady state. We see from figure 1 that plasma parameters become steady state at $t = 9.5$ s as expected, with $T_e(0)$, $T_i(0)$ and $n_e(0)$ remaining constant there after. The time $t \geqslant 9.5$ s was chosen as the initial time for simulating the ICRH driven He^3 ion energy distribution function using the SELFO code and subsequently the NES driven suprathermal tail of the deuterium ion energy distribution function using the FPP-3D code.

3. Inclusion of NES into the FPP-3D code and calculation of LID of ions

The 3D Fokker–Plank equation for the deuterium ion energy distribution function, f_d^0, using a 3D collision operator that includes NES with He^3, has the form [2, 5, 17]

$$\frac{\partial f_d^0}{\partial t} = \frac{v_c^3}{\tau_c} \sum_{n=1,4,5} \frac{1}{\langle 1 \rangle} \frac{\partial}{\partial \bar{x}^n} \left[\sum_{m=1,4,5} \left(A_{nm} \frac{\partial f_d^0}{\partial \bar{x}^m} \right) + B_n f_d^0 \right] + \bar{S}_d - \frac{f_d^0}{\tau_{d,loss}}. \quad (1)$$

The equation is drift trajectory averaged, and it includes drag and diffusion in velocity space, neoclassical ion transport, pitch-angle scattering and Coulomb collisions with the

majority plasma ions and electrons which are both Maxwellian. Collisions amongst the minority He^3 ions are neglected, self-collisions are low due to their high energy and low density. The term $\bar{S}_d$ is the trajectory averaged NES source strength in constants of motion space

$$\left(\bar{x}^1, \bar{x}^4, \bar{x}^5\right) \equiv (\gamma_0, v_0, \vartheta_0),$$
$$\bar{S}_d(t, \gamma_0, v_0, \vartheta_0) = \frac{\langle S_d \rangle}{\langle 1 \rangle},$$

where $S_d = S_d(t, \gamma(\gamma_0, \xi, v_0, \vartheta_0), \xi, v(\gamma_0, \xi, v_0, \vartheta_0), \vartheta(\gamma_0, \xi, v_0, \vartheta_0))$ is the local NES source strength per unit 6D phase space, $\gamma_0 \equiv \bar{x}^1$ is the half-width of the magnetic flux surface at the reflection point for trapped particles or at the innermost point of the trajectory for passing particles, $\vartheta_0 \equiv \bar{x}^5$ is the pitch-angle at the outermost point of the trajectory, $\langle 1 \rangle$ is the trajectory averaged Jacobian representing the transformation from Cartesian to the constants of motion coordinates $\bar{x}^n$ and $v_0 \equiv \bar{x}^4$ is the generalized speed appropriate to the sum of kinetic and potential energies, i.e. $m_d v_0^2/2 = m_d v^2/2 + e_d \Phi(\gamma, \xi)$, where Φ is electrostatic potential, which is taken to be zero in the problem considered here.

The NES source S_d, given by equation (11) in [2], can be written in a form more suitable for numerical calculations

$$S_d(t, \gamma, \xi, v, \theta) = \frac{8\gamma_d^2 n_d(t, \gamma)}{v} \int_{\gamma_d v}^{+\infty} \frac{d\sigma(v_\alpha)}{d\Omega} v_\alpha dv_\alpha \int_0^\pi f_\alpha(t, \gamma, \xi, v_\alpha, \vartheta_\alpha(\chi)) du. \tag{2}$$

with the subscript α denoting the projectile ion, He^3 ions in the case of He^3 minority ICRH and He^4 when we shall treat DT fusion alpha-particles. Other notations read:

$$\gamma_d = (m_d + m_\alpha)/(2m_\alpha),$$
$$\vartheta_\alpha(\chi(v, v_\alpha, \vartheta, u)) = \arccos(\cos\psi \cos\vartheta - \cos u \sin\psi \sin\vartheta),$$
$$\psi = (\pi - \tilde{\vartheta}(\gamma_d, v, v_\alpha))/2, \psi \in [0, \pi/2],$$
$$\tilde{\vartheta} = 2 \arcsin(\gamma_d v/v_\alpha), \tilde{\vartheta} \in [0, \pi/2].$$

The main advantage of representing the source in the form of equation (2) is the constant limits in the internal integral, which result in a uniform numerical error of the corresponding discrete representation. Also, it is clear that the internal integral does not depend on the pitch-angle ϑ if the energy distribution function of projectile ions is isotropic in pitch-angle. We conclude that when the ions α are isotropic the NES source is independent of ϑ_α, a conclusion that was not obvious from the original form the source term in [2].

The differential cross-section for NES of projectile He^3 ions on deuterium target ions, $d\sigma/d\Omega$, is obtained from the data in [15]. Figure 19 of this reference shows the average reaction rate $\sigma_{NI} v_\alpha$ as a function of energy of the He^3 ions E_α in the laboratory frame of the target deuterium. Figure 4 shows the reaction rate in the energy range of interest in this paper. The dependence of the NES cross-section on energy is close to linear. The non-averaged differential cross-section $d\sigma/d\Omega$ can be approximated as in equation (13) in [15]

$$\frac{d\sigma}{d\Omega} \approx \frac{\sigma_{NI}}{4\pi}.$$

Then, according to figure 4, the energy dependence of $v_\alpha d\sigma/d\Omega$ in the source strength in equation (2) is also close to linear. Finally, we note that due to the assumption $E_\alpha \gg E_{d,thermal}$ applied while deriving the expression for S_d in [2], the value $d\sigma/d\Omega$ should be considered a function of the He^3 ion energy before the elastic collision, i.e.

$$\frac{d\sigma}{d\Omega}(E_\alpha) = \frac{d\sigma}{d\Omega}\left(\frac{v_\alpha^2 m_\alpha}{2}\right). \tag{3}$$

The unperturbed deuterium ion density is used in the NES source and in the Coulomb collision operator describing collisions between He^3 ions and majority deuterium ions. The loss term in equation (1) models the direct loss of ions crossing the last closed magnetic flux surface due to the drift deviations of the trajectories from the magnetic flux surfaces. In JET simulations the loss time, $\tau_{d,loss}$, is taken as half of the time required for the ion to complete the trajectory in the projection on the poloidal section of the plasma. Ripple losses in JET plasmas are negligible and ignored in the considerations here. Also ignored are the prompt loss of energetic NES driven deuterium ions and projectile He^3 ions, NES amongst He^3 ions and suprathermal deuterium tail ions and self-collisions amongst deuterium tail ions and amongst the He^3 ions.

In calculating the NES driven deuterium ion energy distribution function the following boundary conditions are used: (i) a Maxwellian distribution function is taken at the boundary $v_0 = v_{0,\min}$ with $v_{0,\min}$ corresponding to the ion temperature. This is valid since NES has a negligible effect on the bulk plasma as mentioned in the previous paragraph; (ii) at the plasma boundary, $\gamma_0 = \gamma_{0,\max}$, the distribution function of He^3 ions is close to zero and the source strength S_d is close to zero too, providing either a Maxwellian distribution of deuterium, or zero deuterium net flux depending on the plasma boundary model; (iii) at $v_0 = v_{0,\max}$, $\vartheta_0 = 0, \pi$ and $\gamma_0 = \gamma_{0,\min}$, zero net flux can be set, since no particles are assumed to go through $v_0 = v_{0,\max}$ (this condition is appropriate to the usual finite treatment of the infinite variation of speed v_0 in a numerical solution of kinetic problems) and the surfaces $\vartheta_0 = 0, \pi$, and $\gamma_0 = \gamma_{0,\min}$ bound the phase space involved in NES interaction.

Extensive tests have shown that in order to obtain acceptably accurate numerical solutions, the kinetic equation (1) should be solved for a perturbed deuterium ion energy distribution function close to a Maxwellian which satisfies equation (1) when the source strength is set $S_d = 0$. A zero initial perturbation to the deuterium distribution was therefore set, while zero boundary condition at $v_0 = v_{0,\min}$ and zero fluxes at all other boundaries were used in the simulation.

The LID of deuterium ions, $\bar{F}_d(t, E)$, corresponding to the NPA measurements on JET with its vertical line-of-sight, is related to the distribution function of all deuterium ions, f_d^0, through

$$\bar{F}_d(t, E) = \sqrt{\frac{2E}{m_d^3}} \int_{Z_p^{(1)}}^{Z_p^{(2)}} f_d^0(t, \gamma_0(\gamma, \xi, v, \vartheta), v_0(\gamma, \xi, v, \vartheta), \vartheta_0(\gamma, \xi, v, \vartheta))\, dZ, \tag{4}$$

where $Z_p^{(k)}$, $k = 1, 2$ are two points of the vertical coordinate Z in JET at which the NPA chord intersects the plasma boundary; $\gamma = \gamma(Z)$, $\xi = \xi(Z)$, $\vartheta = \vartheta(Z)$ are functions of the coordinate along the NPA line of sight. Similarly the LID for other ions which occur in the following simulations, i.e. He^3 ions, DT fusion alpha-particles and other plasma fuel species can be calculated by replacing quantities with subscript d by quantities for the appropriate ions.

In the case of ICRH driven He^3 ions the NES source S_d is intrinsically non-isotropic in pitch-angle. However, it is important to note that only the deuterium ion density enters into S_d, the details of the deuterium ion energy distribution function can be neglected as shown in [2]. This approximation is justified since the energy of the He^3 ions is much greater than that of the thermal deuterium ions, the D ions can be considered to be at rest prior to the elastic collisions.

4. Simulation of ICRH driven minority He^3 ion distribution

Figure 2 illustrates the geometry of the region of ICRH power absorption by the He^3 ions. As already mentioned, $B_\phi(R_{mag}) \approx 3.45\,T$, $I_\phi \approx 1.8\,MA$, $R_{mag} \approx 3\,m$, $\gamma_a \approx 0.9\,m$, $\kappa \approx 1.5$,

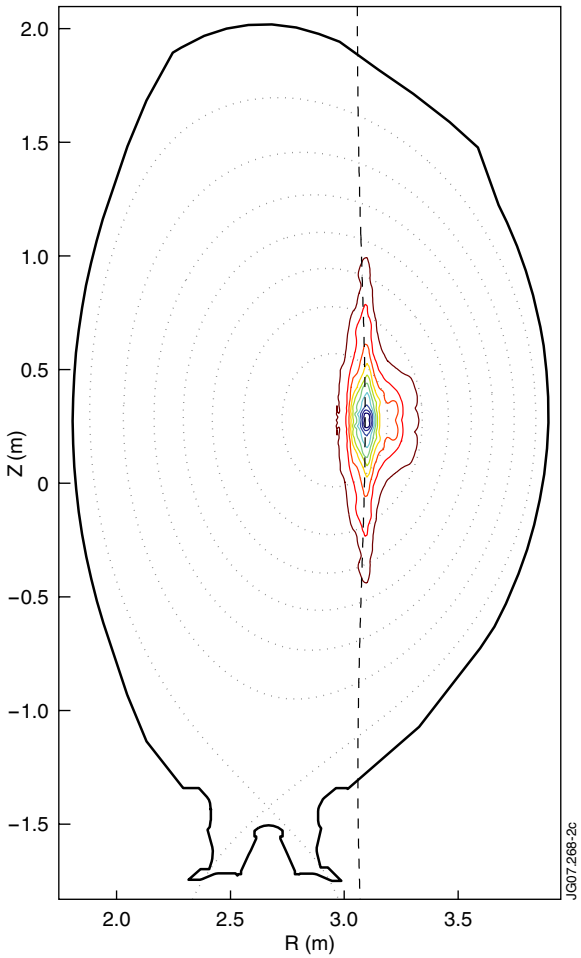

Figure 2. Poloidal cross-section of the plasma at $t = 9.5$ s into JET pulse #53810. The SELFO code calculation of location in the (R,Z) plane of the region of ICRH power absorption by minority He^3 ions in deuterium plasma is shown. Here, $R_{mag} \approx 3$ m, $R_{ICRH} = 3.08$ m, the vertical NPA line-of-sight at $R_{NPA} = 3.07$ m. The plasma configuration shown is representative of pulses #53800, #53801, #53807, #53809, #53810 and #53811, which are the subject of modelling in this paper.

$R_{ICRH} \approx 3.08$ m and $R_{NPA} = 3.07$ m. Two options were used for computing the ICRH driven minority He^3 ion energy distribution function for incorporation into the FPP-3D simulations. The SELFO code yields the ICRH driven He^3 ion energy distribution function in great detail; it is accurate but cumbersome to implement and was therefore used only in the final simulation. For extensive preliminary qualitative studies an analytic energy distribution function based on the formalism described in [21] is better suited.

4.1. SELFO code calculation

The computation of detailed He^3 ion energy distribution function was performed using the SELFO Monte-Carlo code [20] which solves for the global wave field of the fast magnetosonic wave in a deuterium plasma containing the minority He^3 ions with a self-consistent ion energy

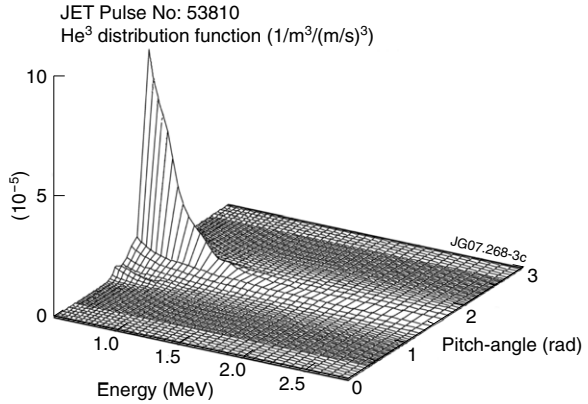

Figure 3. The SELFO code calculation of the He^3 ion energy distribution function at $t = 9.5$ s, on flux-surface with $\gamma = 0.5$ m, at poloidal angle $\xi \approx \pi/2$ (top of the flux-surface), shown as a function of ion energy and pitch-angle. Clearly, the majority of the He^3 ion population is at energy $E < 1$ MeV and peaked at pitch-angles ϑ around $\pi/2$.

distribution function, such that the wave damping is balanced by the ICRH acceleration of the He^3 ions. The SELFO code models the distribution functions of the He^3 ions using an orbit averaged Fokker–Planck equation including Coulomb collisions and quasi-linear interactions with the fast magnetosonic wave. Although this equation is solved using the Monte-Carlo technique the test-particle distribution is mapped onto a finite grid, thus generating a relatively smooth ion energy distribution function

$$f_\alpha^0 = f_\alpha(\gamma, \xi, v, \vartheta).$$

Here α stands for He^3 ions, γ is the half-width in the equatorial plane of the poloidal magnetic flux surface (γ is a label of the flux surface), ξ is the poloidal angle, v is the velocity and ϑ is the pitch-angle. The SELFO code was run with different numbers of He^3 ions in order to assess the smoothing required in these Monte-Carlo calculations for the best representation of the He^3 ion energy distribution function. Figure 3 illustrates the SELFO calculated steady-state He^3 ion energy distribution shown as a function of ion energy and pitch-angle. SELFO also yields the volume averaged ICRH power density $\langle P \rangle$ which we make use of, as explained later in this section, for deriving a simple analytic expression for the He^3 ion energy distribution function.

Interaction of the minority He^3 ions with the ICRH field increases mainly the ion velocity component perpendicular to the magnetic field. The result of the interaction is that the minority He^3 ion energy distribution function is strongly anisotropic in velocity, and the population consists mainly of ions trapped on banana orbits having their turning points close to, but slightly to the high field side of, the non-Doppler shifted ion cyclotron resonance. The NPA measures ions with their turning point on the vertical line-of-sight, i.e. trapped ions with pitch angle $\approx \pi/2$ as explained in [3, 6], matching the condition of the He^3 ions. Moreover, in the measurements discussed in this paper the NPA line-of-sight and the ICRH resonance layer overlap.

4.2. Analytic calculation

In the analytic approach developed in [21], a steady-state energy distribution function for the minority ICRH driven ions is derived, characterized by a 'tail temperature'. For the so-called

perpendicular energy distribution function (pitch-angle ϑ is close to $\pi/2$) equation (38) of [21] gives the following expression for the tail temperature.

$$T_{\rm tail} = T_{\rm e}\left(1+\tfrac{3}{2}\xi\right)/g, \tag{5}$$

$$g = 1 + \frac{R_j((2A+A_j)(2+3\xi)T_{\rm e} - 4AT_j)}{2AT_j(2+2R_j+3\xi)}H(E/E_j),$$

$$E_j = \frac{AT_j}{A_j}\left(\frac{2+2R_j+3\xi}{2\varepsilon(2+3\xi)}\right)^{2/3},$$

$$H(x) \equiv \frac{1}{x}\int_0^x \frac{{\rm d}u}{1+u^{1.5}},$$

where $E = mv^2/2$ is the ion energy, $R_j = n_j Z_j^2 l_j/(n_{\rm e} l_{\rm e})$, $l_j = \sqrt{m_j/(2T_j)}$ is the inverse of the thermal velocity of the majority ion species j, $\varepsilon = 2/(3\pi^{3/2})$, A and A_j are atomic masses of the ICRH driven minority ions and the majority ions, respectively, which have charges $Z|e|$, $Z_j|e|$ and masses m and m_j. $T_{\rm e}$, $T_{\rm i}$ are the temperatures of electrons and majority ions, and $n_{\rm e}$, $n_{\rm i}$ are their densities. The parameter ξ expressed in SI units is

$$\xi = (4\pi\varepsilon_0)^2 \frac{m\langle P\rangle}{8\sqrt{\pi}n_{\rm e}nZ^2{\rm e}^4\ln\Lambda}\left(\frac{2T_{\rm e}}{m_{\rm e}}\right)^{1/2}.$$

Here $\langle P\rangle$ is the volume averaged ICRH power density, n is the density of the minority ions, $\ln\Lambda$ is the Coulomb logarithm and e is electron charge. Equation (5) is valid for high perpendicular energies and strongly anisotropic pitch-angle distribution functions satisfying

$$\frac{m(v\sin\vartheta)^2}{2} > \frac{14.8}{4^{2/3}}T_{\rm e}\left(\frac{2A^{1/2}}{n_{\rm e}}\sum_j n_j Z_j^2\right)^{2/3}.$$

For isotropic distribution functions, the factor 3/2 in equation (5) should be removed. Using equation (5) the following expression for the He^3 ion energy distribution function can be derived:

$$f_{\rm He^3} = C_{\rm norm} n_{\rm He^3}\left(\frac{m_{\rm He^3}}{2\pi T_{\rm He^3,Joule}}\right)^{3/2}\exp\left(-\frac{E_{\rm Joule}}{T_{\rm tail,Joule}}\right)\exp\left(-\left(\frac{\vartheta-\pi/2}{\Delta_\vartheta}\right)^2\right), \tag{6}$$

where $C_{\rm norm}$ is a normalization constant, $\Delta_\vartheta \approx 0.13$ and the label '*Joule*' shows the units used.

The formalism developed in [21] is not tokamak specific, it gives no consideration to non-uniform magnetic fields, trapped ions and other details which we need in simulating ICRH in JET plasmas. Equation (6) describes a spatially local ion energy distribution function, and ignores motion of the energetic He^3 ions over large trajectories during the Coulomb collision time scale. Large deviations of drift ion trajectories from the flux surfaces redistribute spatial ICRH power absorption, mainly by broadening the width of the ICRH resonance layer. In order to include this effect, equation (6) is averaged over drift trajectories using the same technique as for equation (1). Finally, since [21] does not consider the details of the spatial variation of the distribution function of ICRH driven ions, we adjust the constant $C_{\rm norm}$ in equation (6) in order to obtain a simulated LID of the drift trajectory averaged He^3 ion distribution function close to the LID deduced from the NPA measurements at the mid-range of energy, $E \cong 1$ MeV.

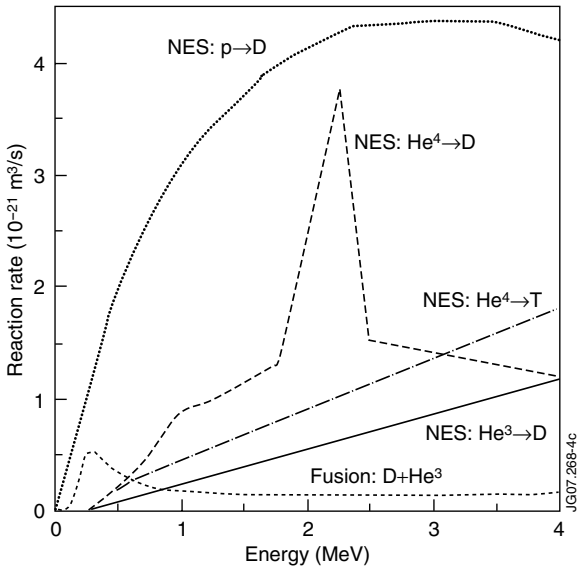

Figure 4. Rate coefficients for NES collision for different (projectile → target) ion combinations which occur in this paper. They are $He^4 \rightarrow D$, $He^4 \rightarrow T$, $He^3 \rightarrow D$ and proton $p \rightarrow D$. The rate coefficients are shown as functions of projectile ion energy, the target ion at rest. Also shown is the rate coefficient for $D + He^3$ fusion reactions in the centre-of-mass frame.

5. FPP-3D computation of NES driven deuterium ion distribution function

The FPP-3D code solves equation (1) in plasmas containing three ion species with quite different energy distributions; initially spatially homogeneous deuterium ions with a Maxwellian energy distribution function which is isotropic in velocity space, initially spatially inhomogeneous He^3 ions with a non-Maxwellian distribution which is anisotropic in velocity space and the spatially inhomogeneous suprathermal NES driven deuterium ions which are also anisotropic in velocity space. In the JET simulation presented here, the FPP-3D code computes the NES driven suprathermal tail of the deuterium ion energy distribution function, the LID of the suprathermal deuterium tail and also the LID of ICRH driven He^3 ions, the latter two for comparison with the NPA measurements.

Using the calculated steady-state He^3 ion energy distribution function from the SELFO code as an input, the drift trajectory averaged energy distribution functions for the He^3 ions and the NES driven suprathermal tail of the deuterium ions was calculated using the FPP-3D code; the calculation was performed for a time interval long enough to obtain steady-state distributions. Figure 4 shows the rate coefficients for NES collisions for different projectile and target ion combinations which are pertinent to this paper. For comparison the rate coefficient for ($D + He^3$) fusion is also shown. Later on in the discussion we shall see the importance of the last process in the analysis of our He^3 ICRH experiments in JET and for similar future heating of ITER plasmas. Figure 5 presents the computed source S_d, integrated over angular and velocity phase space, plotted against the normalized magnetic flux, γ/γ_a. Here, γ is a flux-surface label measured in metres—the half-width of the surface in the equatorial plane, where γ_a is the label of the plasma boundary. Figure 6 shows the same source S_d integrated over γ, the poloidal, toroidal, gyro- and pitch-angles, plotted against the normalized velocity v. Figures 5 and 6 show that the source S_d does not peak at the origin ($\gamma = 0$ and $v = 0$) because

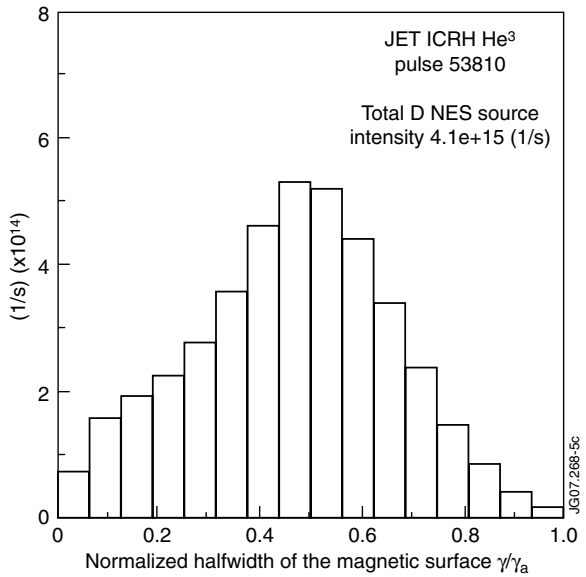

Figure 5. Using SELFO calculated He^3 ion energy distribution as an input, the FPP-3D calculated NES source of deuterium ions is shown at $t = 9.5$ s, integrated over poloidal and toroidal angles and velocity phase space, multiplied by $d\gamma$, plotted as a function of γ. Each bin gives the particle source in $[1/s]$ on the flux-surface γ shown (plasma minor radius $\gamma_a \approx 0.9$ m). The sum over all flux surfaces gives the total NES driven deuterium ion source $S_d = 4.1 \times 10^{15}\ s^{-1}$ in the plasma. This same data, as a function of energy, are illustrated in figure 6.

of the Jacobian in the integrand. Figure 5 also shows that flux surfaces at $\gamma \approx 0.4$–0.6 m contribute most to S_d. Figure 6 shows that the maximum contribution to S_d comes from the region $\nu = 0.25$–0.65 corresponding to an He^3 ion energy of $E \approx 0.2$–1.3 MeV, while at higher energies, e.g. $E \approx 3$ MeV, the contribution is small. Thus we expect that the main effect of the ICRH driven He^3 ions is a NES driven distortion of the majority deuterium ion energy distribution function at energies $E \leqslant 1$ MeV on flux surfaces with $\gamma \sim 0.5$ m. In comparing the NES driven suprathermal tail of the deuterium ion energy distribution function, due to ICRH driven He^3 ions in the present case and DT fusion alpha-particles in the simulations reported earlier in [5], we should bear in mind two factors. First, we note the large difference in the energy distribution of the projectile ions, the He^3 ion population being mostly at energy $E \leqslant 1$ MeV as seen in figure 3, while the DT fusion alpha-particle source is at 3.5 MeV and the projectile ion population extends in energy from 3.5 MeV to thermal energies. Second, as shown in figure 4, the NES rate coefficients for the two projectile species are vastly different in magnitude. Consequently, the total source S_d due to ICRH driven He^3 ions is much smaller (5 times or more) than S_d due to DT fusion alpha-particles in [5], the other plasma conditions in the two experiments being close.

Figure 7 shows the source S_d at $\gamma = 0.5$ m and poloidal angle $\pi/2$ (at the top of the flux surface) as a function of deuterium ion energy and pitch-angle. Comparing figures 3 and 7 we see that a He^3 ion distribution that is narrow in pitch-angles gives deuterium NES that is wide spread in pitch-angles. This pitch-angle spreading effect may be understood from the behaviour of function ϑ_α in equation (2)

$$\vartheta_\alpha = \arccos(\cos\psi\cos\vartheta - \cos u \sin\psi \sin\vartheta). \tag{7}$$

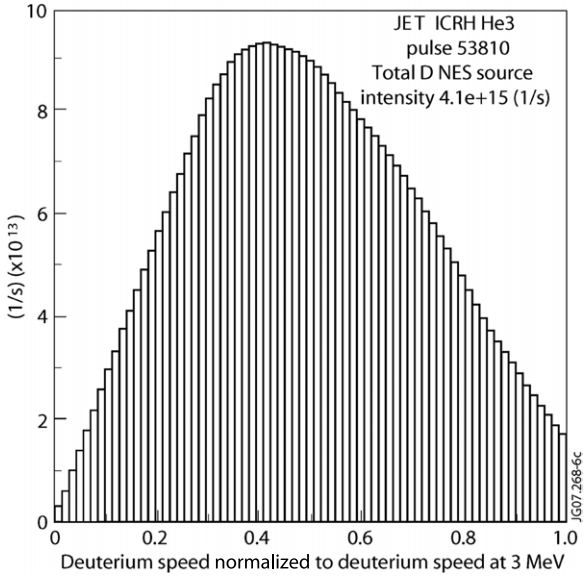

Figure 6. Using SELFO calculated He^3 ion energy distribution as an input, the FPP-3D calculated NES source of deuterium ions is shown at $t = 9.5$ s, as a function of deuterium ion velocity. The source is integrated over γ, the poloidal, toroidal, gyro- and pitch-angles and multiplied by dv. Each bin gives the particle source in $[1/s]$ plotted against ion speed normalized to the speed of a 3 MeV ion. The sum of all bars gives the total deuterium ion source $S_{\mathrm{d}} = 4.1 \times 10^{15}\ \mathrm{s}^{-1}$ in the plasma.

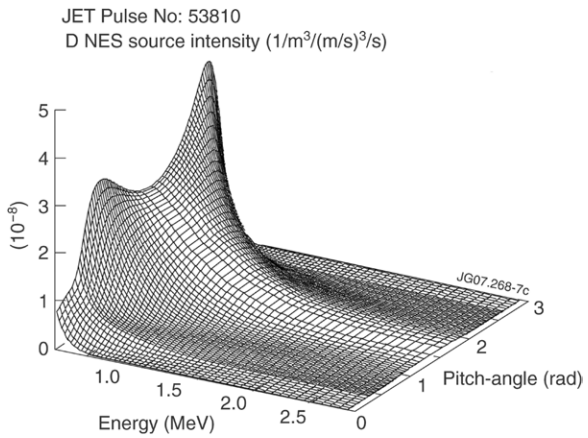

Figure 7. FPP-3D calculated source S_{d} for deuterium ions at $t = 9.5$ s, on the flux surface with $\gamma = 0.5$ m and at poloidal angle $\xi \approx \pi/2$ (top of the flux surface).

Figure 8 shows that while integrating over u in equation (2), values of $\vartheta_\alpha \approx 1.4$–$1.6$ rad, in which the He^3 ion distribution has a strong local maximum (figure 3), are obtained for a wide range of ϑ. Thus, the local He^3 maximum is spreading over a wide ϑ- range in source (2), see figure 7. The width of this ϑ-range decreases as v increases, as seen from cases (a) and (b) in figure 8, and so the width of the source decreases with energy in figure 7.

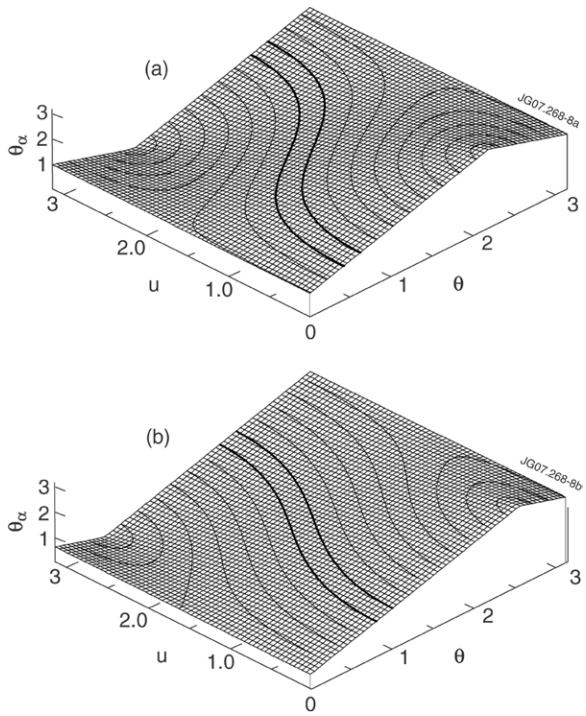

Figure 8. Dependence of θ_α in equation (7) on θ and u. Case (a) is appropriate to $\gamma_d v/v_\alpha \approx 0.55$, case ($b$) to $\approx$0.83. Bold lines are appropriate to $\theta_\alpha = 1.4$ and $\theta_\alpha = 1.6$.

Figures 9(a) and (b) show different projections of the FPP-3D calculated NES driven deuterium ion energy distribution function at $\gamma = 0.5$ m and poloidal angle $\pi/2$ (at the top of the flux surface) plotted against ion energy and pitch-angle. We see that in spite of the relatively wide source S_d the behaviour of the deuterium ion energy distribution function mirrors that of the He^3 ions shown in figure 3, with a maximum around pitch-angle $\vartheta \approx \pi/2$. Large orbit widths play an increasingly stronger role at higher ion energies, as illustrated by figure 9(b). Ions travelling in the direction of the magnetic field reach regions where the source S_d is stronger and therefore show a stronger NES effect. Ions going in the opposite direction sample a smaller source and therefore experience less the effect of NES on He^3 ions. This is due to the spatial localization of the ICRH resonance layer for He^3 (see figure 2) and the deviation of ion drift trajectories to the outer and inner sides of the flux surfaces. Clearly, the trajectory width is an important consideration for the correct calculation of the suprathermal tail of the deuterium ion energy distribution function.

Figure 10 (top graph) shows the LID for He^3 ions inferred from NPA measurements in pulse #53807, compared with LID for He^3 ions simulated using the SELFO and FPP-3D codes. Figure 10 (bottom graph) shows LID for the suprathermal tail of deuterium ions inferred from NPA measurements in pulse #53810, compared with LID for deuterium ions, including the NES on ICRH driven He^3 ions, simulated using the FPP-3D code. Comparing the measured and simulated LIDs shown in figure 10, we conclude that the slopes (or tail temperatures) of the LIDs, especially at higher energies, are in rough agreement with the SELFO+ FPP-3D and FPP-3D simulations. However, the top graph shows that the SELFO + FPP-3D code simulation overestimates the LID for He^3 ions compared with the measured LID for

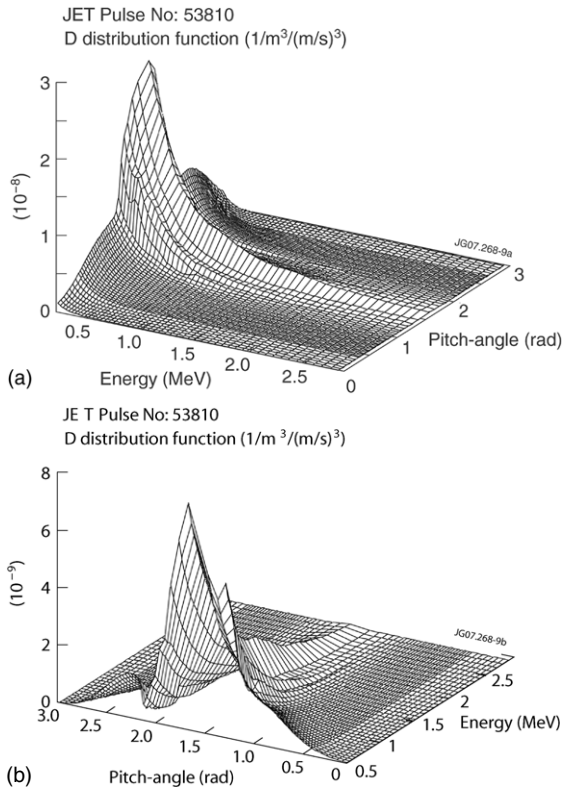

Figure 9. Two sections of the FPP-3D calculated suprathermal tail of the deuterium ion energy distribution function at $\gamma = 0.5$ m and poloidal angle $\pi/2$ plotted against ion energy and pitch-angle.

these ions, whereas the bottom graph shows that the FPP-3D simulation underestimates the LID for the suprathermal tail of the deuterium ion energy distribution function compared to the measured LID for these ions. The excess suprathermal deuterium ion population revealed by the above comparison lies outside the uncertainties in the FPP-3D simulations or in the LID inferred from NPA measurements. In section 6 we discuss an analogous previous comparison between simulation and measurement in JET plasmas where 3.5 MeV DT fusion alpha-particles were the projectile ions, in which the results of the simulation roughly concurred with the measurement. The contrast with the previous comparison reinforces the inference that the observed excess knock-on deuterium population arises due to the interactions of the deuterium ions which are not accounted for in the FPP-3D simulation.

The peak at ≈0.5 MeV in deuterium LID in figure 10 is caused by overlapping of several factors: the energy dependence of the deuterium distribution function, the $\sqrt{E}$ term in formula (4), the deuterium drift trajectory widths, NPA position and localization of the NES source. The location of the peak is appropriate to the maximum of the NES source in figure 6.

6. Simulation of LID of NES driven suprathermal tail of the deuterium ion energy distribution function in JET DT fusion experiments

The main results of measurement and simulation of the NES driven suprathermal tail of the deuterium ion energy distribution function, due to the DT fusion alpha-particles in JET plasmas,

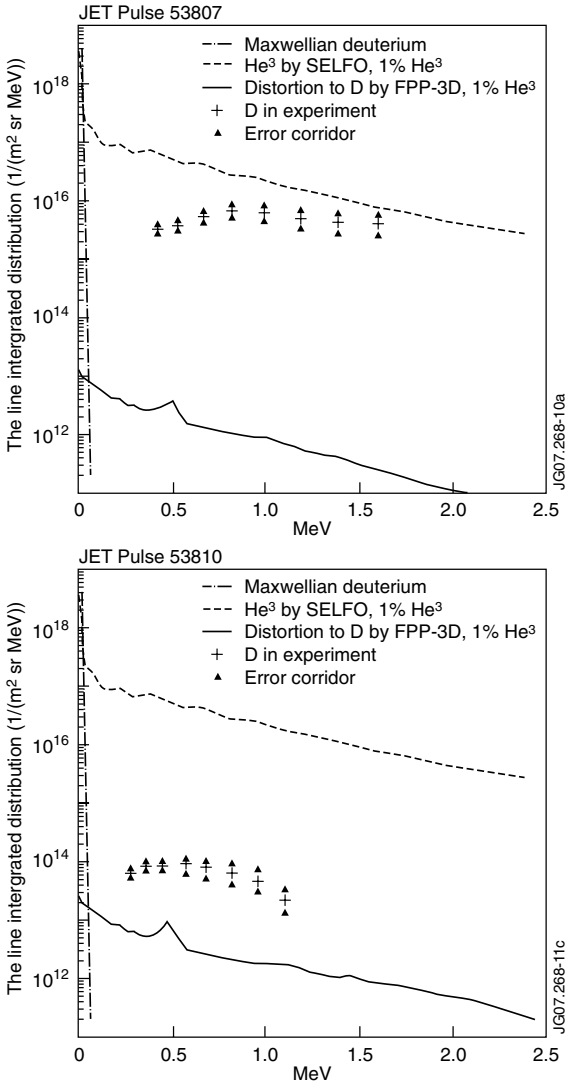

Figure 10. Measured and modelled LIDs at 9.5 s. The top graph is for pulse #53807: the crosses show the LID for He^3 ions inferred from the NPA measurements, the solid upper and lower triangles give the range of uncertainty in the inferred LID. The dashed curve shows the FPP-3D simulation of LID for the He^3 ions using the energy distribution function from the SELFO code. The solid curve shows the FPP-3D simulated LID for the suprathermal tail of the deuterium ion energy distribution function. The bottom graph is for pulse #53810: the crosses show the LID for the suprathermal tail of the deuterium ion energy distribution function inferred from the NPA measurements, the solid upper and lower triangles give the range of uncertainty in the inferred LID. The dashed curve shows the FPP-3D simulation of LID for the He^3 ions using the energy distribution function from the SELFO code. The solid curve shows the FPP-3D simulation of LID for the suprathermal tail of the deuterium ion energy distribution function.

are presented, respectively, in [3] and [5]. In [3] an analytical solution of a 1D Fokker–Planck equation for the slowing-down energy distribution function of DT fusion alpha-particles is calculated using measured deuterium ion and electron densities and temperatures. Using this alpha-particle energy distribution function, a 1D energy distribution function for the NES

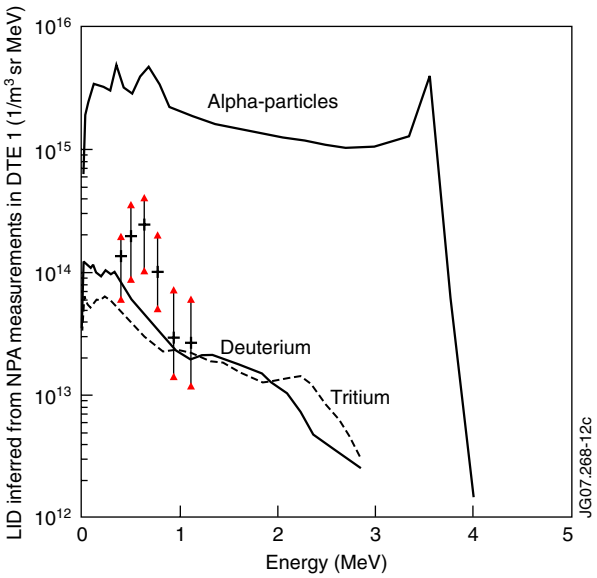

Figure 11. Crosses show the LID of the suprathermal tail of the deuterium ion energy distribution function inferred from NPA measurements presented in figure 6 of [3], the uncertainty in the inferred distribution is shown by the error bars. The measurement is averaged over 0.8 s of the high temperature phase of pulse #42677 of the JET DTE1 experiments. The curves show the FPP-3D simulation, including NES, of LID for the suprathermal tail of deuterium $\overline{F_{\rm d}}$ and tritium $\overline{F_{\rm t}}$ ion energy distribution functions, and also LID for DT fusion alpha-particles $\overline{F_\alpha}$.

driven suprathermal tail of the deuterium ions is calculated, and hence the LID. A comparison between the calculated LID and that inferred from NPA measurements is given in figure 6 of [3], showing reasonable absolute agreement. In [5] a 3D neoclassical transport simulation is performed of the DT fusion alpha-particle slowing-down energy distribution function, of the NES of the alpha-particles on majority deuterium ions, and of the LID of suprathermal tail of the deuterium and tritium ion energy distribution functions. The comparison of the simulated and measured LIDs is shown in figure 11 of this paper. Again, as in [3], credible absolute agreement between the two may be claimed.

At least two important distinctions exist between the simulations of the NES driven suprathermal tail of deuterium ions, due to ICRH driven He^3 ions, on the one hand, and due to DT fusion alpha-particles on the other. In the pulses analysed, the ICRH driven He^3 ion energy distribution function had reached steady state at the time of the LID measurement, whereas the DT fusion alpha-particle, energy distribution function shown in [3] and [5] had insufficient time to do so, due to the premature end of the high temperature phase of the DT plasma. In both cases we expect that for the suprathermal deuterium ion population to reach maximum density, a period of time must elapse, after the plasma has reached steady state, that is of the order of the slowing-down time of the projectile and target ion species. This condition was met in the He^3 experiments and was not in the DT fusion alpha-particle experiments. From a reassessment of the previous simulation of NES due to DT fusion alpha-particles in JET DTE1 plasmas, we expect that if the alpha-particle energy distribution function had reached steady state in the DTE1 plasmas the NES driven suprathermal tail of the deuterium ion energy distribution function would have been about a factor 10 larger in magnitude than that measured and reported in [3].

7. Conclusions

A formalism for calculating the effects of NES of ICRH driven MeV energy He^3 minority ions on majority deuterium ions was incorporated in the FPP-3D neoclassical transport code with JET geometry. With the FPP-3D code, using the SELFO calculation of the energy distribution function of ICRH driven He^3 minority ions as input, the LID of the suprathermal tail of the deuterium ion energy distribution was simulated. The simulation result was compared with the LID of the same ions inferred from NPA measurements. The comparison showed that the measured suprathermal tail of deuterium ions is an order of magnitude larger than that given by the simulation.

The above result was contrasted with analogous previous comparisons presented in [3] and in [5], between NPA measurement of the suprathermal tail of the deuterium ion energy distribution function driven by NES on DT fusion alpha-particles and simulation of this quantity using the FPP-3D code. The previous comparisons between measurement and simulations showed no significant discrepancy between the two, lending credibility to the measurement and simulation.

We infer from the above comparisons and contrasts of the two experiments that the observed excess suprathermal deuterium ion population arises from additional interactions of the ICRH driven He^3 ions which are not accounted for in the FPP-3D simulation. The most plausible candidate for this is the (He^3+D) fusion reaction. Looking at the He^3 ion energy distribution function in figure 3, and the energy dependence of the (He^3+D) fusion rate coefficient in figure 4, we estimate that in the plasmas under consideration the (He^3+D) fusion rate will greatly exceed the (He^3+D) NES rate. We conjecture that the products of (He^3+D) fusion, 14.7 MeV protons and 3.6 MeV He^4 ions, are the additional drivers of NES giving the observed excess suprathermal deuterium ions. Investigations of the knock-on tail formation in the presence of several sources of primary energetic ions coupled through the fusion reaction will be a subject of future work.

The investigation reported in this paper and the discussion of the results point to the need, when modelling the total fusion reactivity of ITER plasmas with He^3 ICRH, of taking proper account of NES of (D + He^3) fusion born alpha-particles and protons as additional drivers of suprathermal fuel ions.

Acknowledgments

The authors thank V G Kiptily for important discussions. The work at the UKAEA was funded jointly by the UK Engineering and Physical Sciences Research Council and by EURATOM. The work at the Moscow State University was funded partly by the Russian Foundation for Basic Research under grants 07-07-00064, SS-1349.2003.1. The views and opinions expressed herein do not necessarily reflect those of the European Commission.

References

[1] Ryutov D 1992 *Phys. Scr.* **45** 153
[2] Helander P, Lisak M and Ryutov D D 1993 *Plasma Phys. Control. Fusion* **35** 363
[3] Korotkov A A, Gondhalekar A and Akers R J 2000 *Phys. Plasmas* **7** 957
[4] Källne J *et al* 2000 *Phys. Rev. Lett.* **85** 1246
[5] Zaitsev F S, Akers R J and O'Brien M R 2002 *Nucl. Fusion* **42** 1340
[6] Korotkov A A, Gondhalekar A and Stuart A J 1997 *Nucl. Fusion* **37** 35
[7] McClements K G, Dendy R O and Gondhalekar A 1997 *Nucl. Fusion* **37** 473
[8] Eriksson L-G *et al* 1998 *Phys. Rev. Lett.* **81** 1231

[9] Mantsinen M, Eriksson L-G, Gondhalekar A and Hellsten T 1999 *Nucl. Fusion* **39** 459
[10] Testa D, Core W G F and Gondhalekar A 1999 *Phys. Plasmas* **6** 3498
[11] Testa D and Gondhalekar A 2000 *Nucl. Fusion* **40** 975
[12] Mantisinen M *et al* 2001 *Nucl. Fusion* **41** 1815
[13] Gorelenkov N *et al* 2003 *Phys. Plasmas* **10** 713
[14] Jacquinot J, Sadler G J and the JET Team 1992 *Fusion Technol.* **21** 2254
[15] Perkins S T and Cullen D E 1981 *Nucl. Sci. Eng.* **77** 20
[16] Zaitsev F S, O'Brien M R and Cox M 1993 *Phys. Fluids* B **5** 509
[17] Zaitsev F S 2005 *Mathematical Modelling of Toroidal Plasma Evolution* (Moscow: MAX Press) (in Russian)
[18] Zaitsev F S, Longinov V V, O'Brien M R and Tanner R 1998 *J. Comput. Phys.* **147** 239
[19] O'Brien M R, Cox M, Gardner C A and Zaitsev F S 1995 *Nucl. Fusion* **35** 1537
[20] Hedin J, Hellsten T, Eriksson L-G and Johnson T 2002 *Nucl. Fusion* **42** 527
[21] Stix T H 1975 *Nucl. Fusion* **15** 1063
[22] McKenzie J S, O'Brien M R and Cox M 1991 *Comput. Phys. Commun.* **66** 194
[23] Budny R V *et al* 1992 *Nucl. Fusion* **32** 429 and references therein (see also http://w3.pppl.gov/transp/)